P. S. Majee[1]
Somnath Bhattacharyya[1]
Prashanta Dutta[2]

[1]Department of Mathematics, Indian Institute of Technology Kharagpur, Kharagpur, India
[2]School of Mechanical and Materials Engineering, Washington State University, Pullman, USA

Received July 13, 2018
Revised August 20, 2018
Accepted August 20, 2018

Research Article

On electrophoresis of a pH-regulated nanogel with ion partitioning effects

The electrophoresis of a polyelectrolyte nanoparticle, whose charge condition depends on the salt concentration and pH of the suspended medium as well as the dielectric permittivity difference, is analyzed. The present nonlinear model for the electrophoresis of this pH-regulated polyelectrolyte (PE) particle is based on the consideration of full set of governing equations of fluid and ion transport coupled with the equation for electric field. The Born energy of the ions are incorporated to account for the difference in the dielectric permittivity of the PE and the electrolyte. The governing equations are computed numerically through a control volume approach. The nonlinear effects are highlighted by comparing with the existing linear model as well as results based on the first-order perturbation analysis valid for a weak applied field. The ion partitioning effect arising due to the difference in self energy of ions between the two media, have a strong impact on the mobility of the PE. The ion partitioning effect attenuates the penetration of counterions in the PE, which enhances the electric force and hence, results in a larger mobility of the PE. The nonlinear effects due to the double layer polarization and relaxation are intensified due to the ion partitioning effect. The ion partitioning effect influences the association/dissociation of PE functional group by tuning the hydrogen/hydroxide ions. Present study shows that the ion partitioning effect is profound for higher salt concentration and/or higher volume density of PE functional groups.

Keywords:
Double-layer polarization / Ion partitioning effect / Numerical study / pH-regulated polyelectrolyte

DOI 10.1002/elps.201800291

1 Introduction

The polyelectrolyte (PE) hydrogels consists of a network of crosslinked polymers containing fixed bound charges/charged groups. The PE nanoparticles, termed as nanogels, with diameters in the range of tens to hundreds of nanometers are of broad interest in the fields of colloids and polymer science. Nanogels bearing ionizable functional groups dissociate to create a charge density when immersed in an aqueous medium. The charge density of the gel depends on the solution pH and ionic concentration. The large water uptake of such networks, often 1000 times more than their own weight, is due to the large osmotic pressure caused primarily by the ionic groups in nanogels. Extraordinary swelling capabilities of nano- or microgels and their responses to external stimuli make them useful for a number of applications such as, DNA sequencing [1], drug delivery [2], chemo-electro-mechanical energy converters, artificial muscles, or as chemical and pH sensors [3]. Numerous studies have now evidenced the benefits of using electrophoresis to measure physical properties of charged macromolecules [4]. The electrophoresis of nanogels or microgels has great practical importance as it can mimic the electrophoretic behavior of DNA, biomacromolecules, and synthetic polymers [5]. The theory and computer simulation of electrophoresis of nanogels is a challenge for their high complexity.

A large number of previous analysis [6–11] considered the electrophoresis of PE nanogel bearing a fixed charge density that is uniformly distributed in the gel. Biological entities like DNA, proteins, and amino acids and synthetic particles like charged dendrimers and polymers can be pH dependent [12]. The immobile charge density of these pH-regulated zwitterionic PE nanoparticles, possessing both the anionic and cationic moieties, depends on their functional groups as well as on the solution pH and background salt concentration. Therefore, it is important to account the presence of H^+ and OH^- ions in the solution. Due to their charge-tunable properties, pH-regulated PEs have been proved to be more suitable materials for the controlled ion transport in nanofluidics [13, 14].

Correspondence: Dr. Somnath Bhattacharyya, Department of Mathematics, Indian Institute of Technology Kharagpur, Kharagpur–721302, India
E-mail: somnath@maths.iitkgp.ernet.in

Abbreviations: **CC**, counterion condensation; **DLP**, double layer polarization; **IEP**, isoelectric point; **PE**, polyelectrolyte

Color Online: See the article online to view Figs. 1–8 in color.

The electroosmotic flow (EOF) and counterion penetration within the PE nanogels are responsible for different electrokinetic behavior compared to a rigid particle. Hermans and Fujita [15, 16] obtained an expression for the electrophoretic mobility of a nano/micro-gel, modeled as a porous sphere possessing a fixed volumetric charge density. Ohshima [17] determines the electrophoresis of a PE based on the Donnan potential governed by the fixed charge density of the PE and the bulk ionic concentration of the suspended aqueous medium. These analysis [15–17] are under the thin Debye layer consideration with low charge density and weak applied electric field assumption. The mobility expressions are derived under the linearized Debye-Hückel approximation with radially symmetric Debye layer, which neglects the double layer polarization (DLP) and relaxation effects. The counterion condensation (CC) effect, arising due to the attraction of counterions by the charged PE nanogel, creates a reduction in the effective charge of the nanoparticle yielding a decrement in mobility.

The experimental studies [4] on electrophoresis of polyelectrolyte demonstrate that the mobility depends nonlinearly with the bulk ionic concentration and volumetric charge density of the PE and discrepancy from the linearized solutions particularly at the low ionic concentration is observed. Several authors [11, 18–22] have considered the nonlinear effects due to DLP, relaxation, and CC based on the linear perturbation analysis from the equilibrium condition under a weak applied field and low charge density assumption. These studies show that the nonlinear effects create a retardation to the electrophoresis of the PE. The full nonlinear model based on the Nernst–Planck equation for ion transport has been considered by Bhattacharyya and Gopmandal [23] and found that effects due to DLP and electroosmosis within the nanogel are significant when the Debye layer is on the order of the nanogel radius or when the permeability is high.

The electrophoresis of a pH-regulated zwitterionic polyelectrolyte nanoparticle has been reported by Yeh et al. [5, 12] based on a linear perturbation analysis of the nonlinear Poisson-Boltzmann equation under a weak applied field assumption. These studies show that the consideration of the DLP, which occurs due to the deformation of the ionic cloud around the polyelectrolyte by convection and electroosmosis of the solution, is essential to successfully predict the electrophoretic motion of a pH-regulated PE. These aforementioned studies are based on weak applied electric field assumption along with Boltzmann distribution of ionic concentration. The assumption of equilibrium Boltzmann distribution of ionic species may not be proper for the case of a low background salt concentration (i.e., when the Debye length is of order of the particle radius) and a highly charged PE nanogel.

The flexible PE can assume various shapes when subjected to an external electric field. The average quantities such as the mobility of a nonspherical particle are mostly close to what is found for spherical particles of equivalent volume and charge [24]. For a sufficiently thin Debye layer under the free darning limit, that is each segment of the PE experiences the same drag force, the mobility becomes size independent. Hsu et al. [20] studied the effect of the shape of a PE on its electrophoresis by considering an ellipsoid of different aspect ratio and found that the double layer polarization and relaxation varies with the shape of the PE. A shape change also modifies the counterion condensation of the PE. Duval and his coworkers [25] demonstrated that the consideration of a diffuse PE-liquid interface, instead of a step-like distribution of polymer segments, is more appropriate in the context of analyzing electrokinetics of microorganisms or humic substances. In the diffuse formulation, the interfacial properties of the PE gradually approaches to that of the surrounding aqueous medium. In this study however, we have considered a spherical PE in which the polymer segments and charged sites are uniformly distributed. The influence of the charged parameters on the electrophoresis of a nonspherical PE will be qualitatively similar to that of a spherical PE.

Most of the previous studies have considered the dielectric permittivity of the PE to be the same as that of the adjoining electrolyte solution, which is justified only when the polymer density of the PE is low [26]. Since the dielectric permittivity of the gel is less than that of the surrounding solution, the effective permittivity of the PE is smaller than that of the solution [27]. Young et al. [28] has cited several situations in which the dielectric permittivity of the soft gel is found to be lower than the bulk dielectric constant. Coster [29] has shown that the difference in permittivities creates a growth in the membrane-solution Donnan potential. As the ions prefer to stay in a medium with higher dielectric permittivity, a substantial change in the arrangement of the ions within the PE is expected. This electrokinetic phenomenon is referred to as ion partitioning effect, which arises due to the difference in electrostatic-free energy between the two mediums [29]. López-García et al. [30] numerically investigated the effect of ion partitioning by solving the Poisson-Boltzmann equation for a suspended spherical particle covered by a permeable membrane layer bearing inhomogeneous fixed charge distribution. Based on the Boltzmann distribution of ions, Ganjizade et al. [31] analyzed the impact of the ion partitioning effect on the electrostatic of a soft particle with a volumetrically charged core covered by a pH-regulated polyelectrolyte layer. They observed that if the permittivities of two adjacent media differ, a change in the slope of the electrostatic potential profile at the interface develops. Recently, Maurya et al. [32] studied the ion partitioning effect on electrophoresis of a soft particle through the Debye-Hückel approximation under a thin Debye layer consideration. All these studies [27, 30–32] suggest that the ion partitioning effect is an important electrokinetic phenomenon involving two neighboring media with different dielectric permittivity. Previous studies dealing with the ion partitioning effect on electrophoresis neglected the double layer polarization and relaxation effects thus, valid for the low charge and weak electric field condition with thinner Debye layer assumption.

In the present study, we consider the electrophoresis of a pH-regulated zwitterionic PE nanogel with ion partitioning effects. The PE charge is influenced by the pH and the salt

concentration as well as ion partitioning effect arises due to the difference in permittivity. The dielectric permittivity of the nanogel may become lower than the surrounding aqueous media, which induces the ion partitioning effect. Despite its great relevance on electrokinetics, the impact of the ion partitioning effect on electrophoresis of a nanogel has not been taken into account by any previous researcher. It may be noted that for charged nanogels there is no well-established conversion formula to relate the mobility with its electrostatic property. For a rigid colloid the zeta-potential measurements are normally based on measuring the electrophoretic mobility and converting that back to a surface potential. However, for pH-regulated nanogels neither the Helmholtz model nor the linearized colloidal model [15–17] should be applicable.

To account the effects of EOF of the unbalanced ions, the double-layer polarization and relaxation, and counterion condensation, we numerically solve the full electrokinetic equations governing the flow phenomena. The present mathematical model is based on the coupled set of Navier-Stokes-Nernst-Planck-Poisson equations. The present analysis thus does not invoke a weak electric field or low particle charge assumption. To count for the ion partitioning effect, the Born energy is incorporated in the Poisson equation for electric potential and in hydrodynamics of the ionized fluid within the nanogel. A pressure correction-based control volume approach is adopted to compute the governing equations. Results show that the electrophoretic motion of the particle depends on the physicochemical properties of the particle as well as properties of the solution. We found that the ion partitioning effect causes a significant rise in the electrostatic charge of the nanogel. Ion partitioning effect also increases the magnitude of the electrophoretic velocity and the rate of this increment manifests for the higher effective charge density of the PE. In the present model the effect of the hydrogen and hydroxide ions on the electrophoresis of the pH-regulated PE is taken into account.

2 Mathematical model

We consider the electrophoresis of an ion and fluid penetrable spherical polyelectrolyte (PE) nanogel of radius a with dielectric permittivity ε_p carrying both dissociable acidic and basic functional groups suspended in an electrolyte solution of permittivity ε_e. The structure of the PE is assumed to be homogeneous with a hydrodynamic screening length ℓ. The spherical polar coordinates (r, θ, φ) are adopted with the origin located at the center of the particle and z-axis ($\theta = 0$) is along the imposed electric field E_0 (Fig. 1).

Two media of different dielectric constant creates a difference in the ion concentration as a result of the difference in the electrostatic-free energy of the ions [29]. The difference in concentration n_i of the i^{th} ionic species between the two media due to the difference in free energy of the ion can be related as $n_i(r = a-) = f_i n_i(r = a)$. The ion partition coefficient factor $f_i = \exp(-\Delta W_i/k_B T)$, is obtained with the aid of Boltzmann equation. Here ΔW_i is the change in the

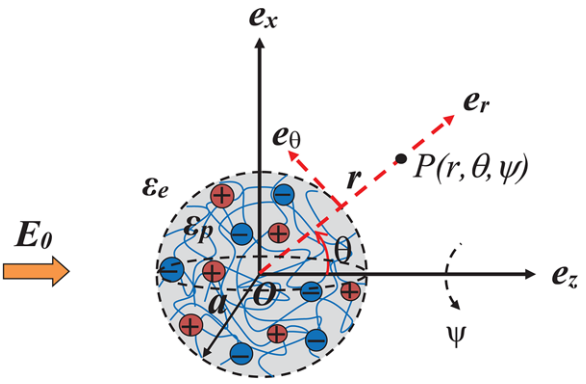

Figure 1. Schematic representation of the electrophoresis of a spherical polyelectrolyte of radius a subject to an applied electric field E_0.

electrostatic free energy when the i^{th} ion goes from a medium of dielectric permittivity ε_e to the one of ε_p, and it can be expressed as [33]

$$\Delta W_i = \frac{(z_i e)^2}{8\pi r_i}\left(\frac{1}{\varepsilon_p} - \frac{1}{\varepsilon_e}\right) \tag{1}$$

Here r_i denotes the radius of the i^{th} ionic species of charge $z_i e$.

The space charge density of the PE depends on the pH and electrolyte concentration as well as the PE-to-electrolyte permittivity ratio. If K_A and K_B are the equilibrium constants of the association/dissociation reactions and N_A and N_B are concentration of acidic and basic functional groups, respectively, then the net charge density ρ_{fix} of the PE can be expressed as [12]

$$\rho_{fix} = -1000F([A^-] - [BH^+]) = -1000F\left[\frac{N_A}{1+\left(\frac{[H^+]_{PE}}{K_A}\right)} - \frac{N_B\left(\frac{[H^+]_{PE}}{K_B}\right)}{1+\left(\frac{[H^+]_{PE}}{K_B}\right)}\right] \tag{2}$$

where F is the Faraday constant and $[H^+]_{PE}$ denotes the molar concentration of H^+ in PE with $[H^+]_{PE} = [H^+]\exp(-\Delta W_i/k_B T)$. In the absence of the electric field, $[H^+]$, $[OH^-]$ obey the equilibrium Boltzmann distribution, and they follow the Nernst–Planck equation when the nanogel is in electrophoresis under an external field.

The hydrodynamic interactions within the PE is analyzed through a continuum framework that adopts the Brinkman model. Thus, the governing equations describing the motion of an ionized fluid within the PE are the Brinkman extended Navier-Stokes equations and outside the PE is governed by the Navier-Stokes equations. We have adopted a single-domain formulation [23] in which the equation of motion in the composite region, consists of the polyelectrolyte region and electrolyte medium, are expressed by a single set of equations with the aid of the unit step function. The advantage of this approach is that no boundary conditions are needed at the fluid-PE interface as this interface is within the computational domain.

The transport of ions is governed by the Nernst–Planck equations, which takes into account the ion flux due to convection, diffusion, and electromigration. The electric potential in the PE and the electrolyte region is governed by the Poisson equation. We scale the dimensional variables as follows: the length scale is the radius of the sphere a, the thermal potential $\phi_0 = k_B T/Ze$ is the scale for the electric potential, $U_0 = \varepsilon_e \phi_0{}^2/a\mu$ is the velocity scale, $\tau = a/U_0$ is the time scale, $\varepsilon_e\phi_0{}^2/a^2$ is the pressure scale, the bulk number concentration n_{i0} is the scale for the ionic concentration of the i^{th} ionic species and $\Lambda = E_0 a/\phi_0$ is the scaled external electric field. Here e is the elementary charge, k_B is the Boltzmann constant, T is the absolute temperature and μ is the dynamic viscosity. The electrophoresis can be considered to be axially symmetric with z-axis as the axis of symmetry. Incompressible Newtonian fluid describing the motion of ionized fluid can be expressed in nondimensional form as [23],

$$Re\frac{\partial \mathbf{u}}{\partial t} + Re(\mathbf{u}.\nabla)\mathbf{u} - \nabla^2\mathbf{u} + \nabla p + \beta^2\mathbf{u}[H(r) - H(r-1)] + \left\{[H(r) - H(r-1)]\exp\left(-\frac{\Delta W}{k_B T}\right) + H(r-1)\right\}(\kappa a)^2\rho_e\nabla\phi = 0 \quad (3)$$

$$\nabla.\mathbf{u} = 0 \quad (4)$$

where $\mathbf{u} = (u, v)$ is the velocity vector, u is the cross radial and v is the radial velocity components, t is the time, p is the pressure, ϕ is the electrical potential and $H(r)$ is the Heaviside step function. The scaled charge density $\rho_e = \sum_{i=1}^{4} n_{i0} z_i n_i / (\sum z_i^2 n_{i0})$, where n_i is the scaled ionic concentration of the i^{th} ionic species with valence z_i. The ionic species correspond to the mobile ions of electrolyte as well as H^+ and OH^- released due to the reaction of gel functional group. If KCl is the background salt, then the corresponding hydrated ionic radii of the ionic species K^+, Cl^-, H^+, and OH^- are 3.31, 3.32, 2.82, and 3.0Å, respectively [35]. For the sake of computational simplicity, we have considered the ionic radius r_i (= 3.3Å) are equal for all the ionic species, which leads to $\Delta W_i = \Delta W$ for all i. The nondimensional parameter $\beta = a/\ell$, provides a measure of the friction experienced by the fluid within the porous layer. Here $Re = U_0 a\rho/\mu$ is the Reynolds number, ρ is the fluid density and $\kappa = \sqrt{\mathcal{Z}^2 e^2 I/\varepsilon_e k_B T}$ is the inverse of the EDL thickness, where $I = \sum_{i=1}^{4} z_i^2 n_{i0}$ is the ionic strength.

The nondimensional Nernst-Planck equation governing the distribution of the i^{th} ionic speicies is

$$Pe_i\frac{\partial n_i}{\partial t} + Pe_i(\mathbf{u}.\nabla n_i) = \nabla^2 n_i + \frac{z_i}{\mathcal{Z}}\nabla.(n_i\nabla\phi) \quad (5)$$

where the nondimensional parameter $Pe_i = \varepsilon_e\phi_0{}^2/\mu D_i$ is the Péclet number of the i^{th} ion, measures the ratio of advective to diffusion transport of ions with D_i being the diffusivity of the i^{th} ion.

The electric potential within and outside the PE is governed by the Poisson equations

$$\nabla^2\phi = -\frac{1}{\varepsilon_r}\left[(\kappa a)^2\exp\left(-\frac{\Delta W}{k_B T}\right)\rho_e + Q_{fix}(r,\theta)\right] \quad (r \le 1) \quad (6)$$

$$\nabla^2\phi = -(\kappa a)^2\rho_e \quad (r > 1) \quad (7)$$

where $\varepsilon_r = \varepsilon_p/\varepsilon_e$ is the PE-to-electrolyte permittivity ratio. The nondimensional form of the immobile charge density of the PE is

$$Q_{fix}(r,\theta) = -\left[\frac{Q_A}{1 + 10^{(pK_A - pH)}\exp(-\frac{\Delta W}{k_B T})[H^+]} - \frac{Q_B 10^{(pK_B - pH)}\exp(-\frac{\Delta W}{k_B T})[H^+]}{1 + 10^{(pK_B - pH)}\exp(-\frac{\Delta W}{k_B T})[H^+]}\right] \quad (8)$$

where $Q_j = FNja^2/\varepsilon_e\phi_0$ (j = A, B) is the maximum charge density due to acidic and basic functional groups, $pK_A = -\log K_A$ and $pK_B = -\log K_B$. Here $[H^+]$ is the nondimensional concentration of H^+ ion scaled by $[H^+]_0$, the bulk molar concentration of H^+ . When $N_A = N_B$, the volumetric charge density of the PE is zero for pH = $(pK_A + pK_B)/2$, which is known as the isoelectric point (IEP).

Far from the particle ($r = R >> 1$)

$$\mathbf{u} = -U_E\mathbf{e_z}, \quad \phi = -\Lambda R\cos\theta, \quad n_i = 1 \quad (9)$$

where U_E is the electrophoretic velocity of the particle. In the present problem, we have considered the frame of reference as fixed at the particle center. With respect to this stationary frame of reference, the particle is experiencing a uniform velocity $-U_E$ at the far field. A radial symmetry condition (i.e., $\frac{\partial X}{\partial r} = 0$ for $X = \mathbf{u}, \phi, n_i$) is imposed at $r = 0$.

The forces experienced by the PE are the electric force and the drag force. The axisymmetric nature of our problem suggests that only the z-component of these forces need to be considered. The electrostatic and hydrodynamic forces along the flow direction can be calculated by integrating the Maxwell stress tensor $\boldsymbol{\sigma}^{\mathbf{E}}$ and hydrodynamic stress tensor $\boldsymbol{\sigma}^{\mathbf{H}}$ respectively, on the surface of the PE and are given by

$$F_E^* = \iint_S (\boldsymbol{\sigma}^{\mathbf{E}}.\mathbf{e_r}).\mathbf{e_z}\,dS \quad (10)$$

$$F_D^* = \iint_S (\boldsymbol{\sigma}^{\mathbf{H}}.\mathbf{e_r}).\mathbf{e_z}\,dS \quad (11)$$

where $\boldsymbol{\sigma}^{\mathbf{E}} = \varepsilon_e[\mathbf{EE} - (1/2)E^2\mathbf{I}]$and $\boldsymbol{\sigma}^{\mathbf{H}} = -p\mathbf{I} + \mu[\nabla\mathbf{u} + (\nabla\mathbf{u})^T]$. Here $\mathbf{E} = -\nabla\phi$, $E^2 = \mathbf{E}.\mathbf{E}$, $\mathbf{EE}$ denotes the vector direct product and $\boldsymbol{I}$ is the unit tensor. The variables with an asterisk in superscript denote the dimensional quantities. The non-dimensional form of force terms are

$$F_E = -\iint_S\left[\frac{\partial\phi}{\partial r}\frac{\partial\phi}{\partial z} - \frac{1}{2}\left\{\left(\frac{\partial\phi}{\partial r}\right)^2 + \left(\frac{1}{r}\frac{\partial\phi}{\partial\theta}\right)^2\right\}\cos\theta\right]dS \quad (12)$$

$$F_D = \iint_S\left[\left\{-p + 2\frac{\partial v}{\partial r}\right\}\cos\theta - \left\{r\frac{\partial}{\partial r}\left(\frac{u}{r}\right) + \frac{1}{r}\frac{\partial v}{\partial\theta}\right\}\sin\theta\right]dS \quad (13)$$

The forces F_E and F_D are scaled by $\varepsilon_e\phi_0{}^2$.

The electrophoretic velocity is unknown a priori, which is obtained by solving the force balance equation $F_E + F_D = 0$ iteratively. The iteration procedure starts with an initial assumption for U_E. Using this U_E, the governing electrokinetic

Table 1. Electrokinetic parameters

Ionic species	K^+	Cl^-	H^+	OH^-
Pe_i [5]	0.238	0.23	0.05	0.088
n_{i0} (pH ≥7)	C_{KCl}-$10^{-pH+3} + 10^{-(14-pH)+3}$	C_{KCl}	10^{-pH+3}	$10^{-(14-pH)+3}$
n_{i0} (pH <7)	C_{KCl}	C_{KCl}-$10^{-pH+3} + 10^{-(14-pH)+3}$	10^{-pH+3}	$10^{-(14-pH)+3}$

Key parameters: $\phi_0 = 0.02586$V, $\varepsilon_e = 695.39 \times 10^{-12}$ C/Vm, $\mu = 10^{-3}$Pa s, and $\rho = 10^3$kg/m^3.

equations are solved through the numerical algorithm as outlined in the following section. Based on the solution of the electrokinetic equations the forces are obtained by Eqs. (12) and (13). The iteration process is repeated till the difference in U_E between two successive iterations becomes smaller than 10^{-6}. The initial guess for U_E is determined through the linear analysis, which we developed following Ohshima et al. [7]. The scaled electrophoretic mobility, scaled by $\varepsilon_e\phi_0/\mu$, is defined as $\mu_E = U_E/\Lambda$.

We have imposed the far-field conditions at $R = 25a$, since further increase in R does not creates any significant change on the drag or electric force on the PE. The capillary diameter in electrophoresis varies between 5 and 100 μm. Thus, the capillary walls may not have a significant impact on the PE electrophoresis. If the capillary size is decreased to nanometers then the mobility of PE is expected to be influenced by the interactions between the EDLs. Thus, the wall effects can safely be ignored for the nanogel electrophoresis.

3 Numerical methods

The governing equations along with the prescribed boundary conditions are solved numerically through a control volume approach over a staggered grid arrangement. The discretized form of the governing equations is obtained by integrating them over each control volume. Different control volumes are used to integrate different equations. The discretized equations are solved through the pressure correction-based iterative SIMPLE (Semi-Implicit Method for Pressure-Linked Equations) algorithm. This procedure is based on a cyclic guess-and-correct operation to solve the governing equations. The pressure link between the continuity and momentum equations are accomplished by transforming the discretized continuity equation into a Poisson equation for pressure correction. This Poisson equation implements a pressure correction for a divergent velocity field. At each iteration the equation for the electric field, i.e. Eqs. (6) and (7) are computed to obtain the potential field. Equations (6) and (7) are computed through the successive-over-relaxation (SOR) technique. A time-dependent numerical solution is achieved by advancing the variables through a sequence of short time steps. We start the motion from the initial stationary condition and achieve a steady-state after a large time step for which the variables become independent of time.

A computer code is developed based on the algorithm as outlined above. The developed computer code is tested for accuracy by comparing with existing experimental as well as theoretical analysis, which has been discussed subsequently.

4 Results and discussion

We consider an aqueous dispersion of amino acid PE nanogel of radius $a = 10$ nm, $pK_A = 2.5$ (α-carboxyl), and $pK_B = 9.5$(α-amino) [34] with IEP = 6.0 when $N_A = N_B$. The variation of N_A (and N_B) is considered in the similar range as indicated by Yeh et al. [12] for biopolyelectrolytes. We consider the electrolyte as an aqueous KCl solution at $T = 298$ K and the solution pH is adjusted by KOH and HCl. The mobile ions are H^+,K^+, Cl^-, and OH^-, the concentrations of which are normalized by the bulk values $[H^+]_0$, $[K^+]_0$, $[Cl^-]_0$, $[OH^-]_0$, respectively. If C_{KCl} be the concentration of the background salt KCl, then following Yeh et al. [12] the bulk concentration of ions based on the electroneutrality condition can be expressed as provided in Table 1. Our numerical results demonstrate that the inertial terms in the momentum equations have no significant impact when the particle size a is in the nanometer range. We have however retained these terms as the present numerical algorithm for fluid flow is based on the unsteady formulation.

4.1 Distribution of Q_{fix} when $E_0 = 0$

If IEP, the pH at which the net electric charge due to dissociation/association of the ionizable groups in the PE is zero, is larger (smaller) than pH then the PE becomes positively (negatively) charged. In absence of the externally applied electric field, the distribution of the fixed charge density in the PE shows no angular variation. The distribution of fixed charge density along the $\theta = 0$ line at different pH is shown in Fig. 2A. As the concentration of H^+ ions decreases with the increase of pH, more number of negative charge dissociates from the PEL functional group leading to a negative volumetric charge density at a higher pH. The bulk ionic strength also increases as pH deviates from 7.

Figure 2B shows the distribution of fixed charge in PE along the line $\theta = 0$ at a fixed pH for different values of the salt concentration. Under the same pH the volumetric charge density of the PE increases with an increase in the background salt concentration. This has been explained in details by Yeh et al. [12]. For pH < IEP, the PE is positively charged and it increases with the increase of the salt concentration. On the other hand for pH > IEP, the

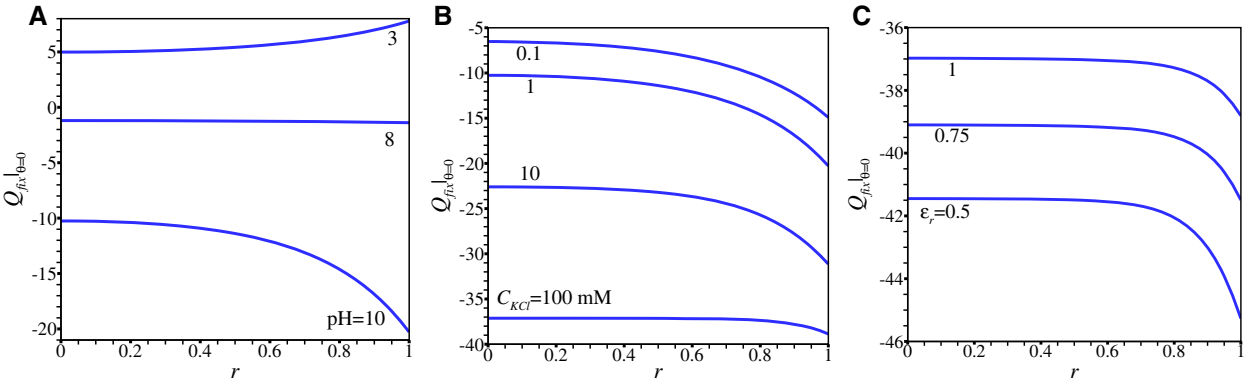

Figure 2. Radial distribution of fixed charge density within the nanogel along the line $\theta = 0$ in absence of the applied electric field ($E_0 = 0$) for (A) different pH (= 3, 8, and 10) at $C_{KCl} = 1$ mM with $\varepsilon_r = 1$; (B) different C_{KCl} (= 0.1, 1, 10, and 100 mM) at pH = 10 with $\varepsilon_r = 1$; and (C) different ε_r (= 0.5, 0.75, and 1) at $C_{KCl} = 100$ mM with pH = 10, when $N_A = N_B = 100$ mM.

concentration of H^+ inside the PE is smaller than outside of it. An increase in salt concentration decreases the concentration of H^+, which creates an increment in negative charges in the PE.

Figure 2C shows that the immobile charge of PE is larger when PE-to-electrolyte permittivity ratio ε_r is low. If the permittivity of the PEL is less than that of the electrolyte, the hydrogen/hydroxide ions prefer to remain inside the electrolyte, which leads to a lower concentration of H^+ in PE. A lower accumulation of H^+ ions in PE leads to a more ionization of PE functional group, which creates a larger PE charge.

4.2 Validation with experimental data and theoretical analysis for mobility

In order to verify the accuracy of present algorithm we have computed the mobility in absence of the ion partitioning effect ($\varepsilon_r = 1$) and compared with the experimental results of Duval et al. [35] for the electrophoresis of a succinoglycan biopolyelectrolyte of radius 10.8 nm suspended in an aqueous NaCl solution at bulk pH = 10.3. As the PEL is succinoglycan, $pK_A = 4.58$, $pK_B = 8.6$ and the background salt is NaCl, $Pe(Na^+) = 0.351$, $Pe(Cl^-) = 0.23$. Figure 3A shows that the present numerical solutions are in very good agreement with the experimental results of Duval et al. [36].

Yeh et al. [12] determined numerical solution for the mobility based on the first-order perturbation analysis from the equilibrium Boltzmann distribution of ions. Figure 3B and C shows that our computed solutions for mobility with $\varepsilon_r = 1$ are in good agreement with the solutions due to Yeh et al. [12].

4.3 Double layer polarization and counterion condensation

For the pH-regulated PE, the volumetric charge density increases with the increase of salt concentration when the difference between the bulk pH and IEP is large. Results (Fig. 3A–C) show that the variation of mobility with the bulk ionic concentration of salt depends on the concentration of the PE functional group and pH. We find that μ_E varies nonlinearly with C_{KCl} and approaches a constant at a larger value of C_{KCl}. While the mobility of a rigid particle approaches zero as the ionic strength is increased, mobility of a PE instead approaches a finite limiting value. The accumulation of mobile counterions within the PE attains a saturation when ionic concentration of the electrolyte medium becomes sufficiently large and the mobility can be obtained based on the balance of Stokes drag and electric force of individual monomers constituting the PE [7]. Similar trend in the mobility is observed (Fig. 3B) for the pH-regulated PE. For $\kappa a \sim O(1)$, mobility increases with the increase of κa till it attains a local maximum and then mobility decreases and approaches a constant for $\kappa a >> 1$. The occurrence of the local maximum in the mobility indicates the onset of the double layer polarization (DLP) effect beyond this κa. The polarization of double layer creates a retarding electric force, which attenuates the growth of mobility with κa. The DLP effect is significant for a thick Debye length, i.e. $\kappa a \sim O(1)$ [23]. Mobility starts decreasing with C_{KCl} when the shielding effect on the immobile charge of PE becomes strong, which reduces the effective charge of the PE and hence the mobility. In addition, at a large bulk ionic concentration the counterion condensation (CC) occurs, which creates a saturation of mobile counterions within the PE. This leads to the μ_E become invariant with further increment in C_{KCl}. The occurrence of CC depends on the charge density of PE. For larger range of N_A, a larger value of C_{KCl} is required for the onset of CC. Similar variation of μ_E of a fully dissociated PE due to the variation of the bulk ionic concentration is found by Yeh et al. [37].

To illustrate the PE charge neutralization and the occurrence of CC we have determined the neutralization factor Γ defined as:

$$\Gamma = 1 - \frac{Q_{eff}}{\bar{Q}_{fix}} \tag{14}$$

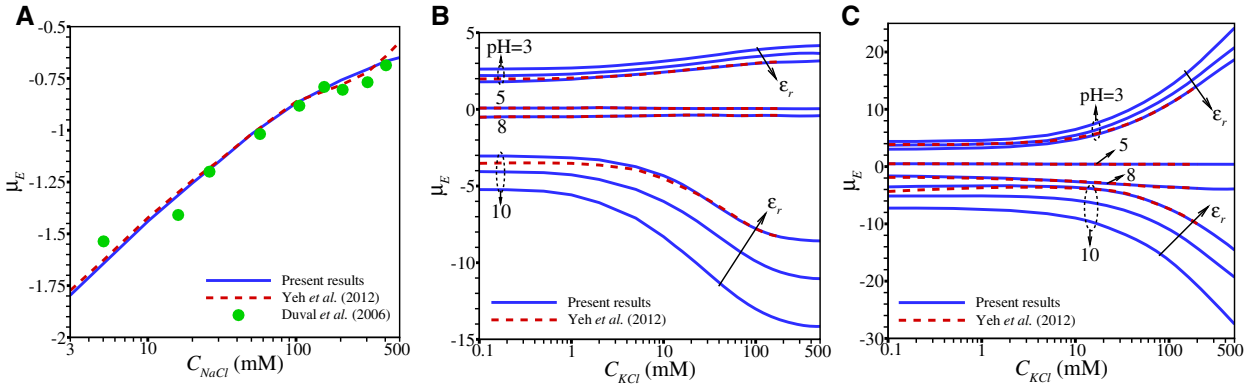

Figure 3. (A) Comparison of our computed electrophoretic mobility for $\varepsilon_r = 1$ with the experimental results of Duval et al. [36] as a function of salt NaCl concentration, radius of the PE $a = 10.8$ nm, pH = 10.3, p$K_A = 4.58$, p$K_B = 8.6$, $N_A = 213$ mM, $N_B = 26$ mM, $\ell = 0.635$ nm, and $E_0 = 10^4$ V/m. Variation of mobility with C_{KCl} for (B) $N_A = N_B = 100$ mM and (C) $N_A = N_B = 900$ mM for different ε_r (= 0.5, 0.75, 1) and different pH (= 3, 5, 8, 10) when p$K_A = 2.5$, p$K_B = 9.5$, and $\beta = 2$. Dashed red lines correspond to the numerical results of Yeh et al. [12].

where the volume-averaged effective charge density (Q_{eff}) and volume-averaged fixed charge density ($\bar{Q}_{fix}$) within the nanogel are determined as:

$$Q_{eff} = \frac{3}{2}\int_{r=0}^{1}\int_{\theta=0}^{\pi}\left[(\kappa a)^2 \exp\left(-\frac{\Delta W}{k_B T}\right)\rho_e + Q_{fix}\right] r^2 \sin\theta dr d\theta, \quad (15)$$

$$\bar{Q}_{fix} = \frac{3}{2}\int_{r=0}^{1}\int_{\theta=0}^{\pi} Q_{fix} r^2 \sin\theta dr d\theta. \quad (16)$$

The shielding effect depends on the permeability of the PE. If the PE is highly permeable, the EOF due to the mobile counterions within the PE becomes stronger and the charge neutralization delays. As the PE become less permeable, the diffusion dominated shielding effect grows and the convective transport of the mobile counterions slows down, which in combination produces an enhancement in charge neutralization factor, i.e. increment in Γ. The distribution of Γ as a function of κa shows that it increases rapidly with the increase of C_{KCl}. The rate of increment in Γ reduces at a higher range of C_{KCl} and approaches a constant when the CC effects dominates. For sufficiently thin Debye length ($\kappa a >> 1$), the mobility should approach to a constant Q_{fix}/β^2, the electrophoretic mobility of an individual polymer segment.

The mobility dependence of pH (Fig. 3B, C, and Fig. 4B) shows that the absolute value of the mobility increases as pH deviates from the corresponding IEP. The mobility dependence on salt concentration and the concentration of PE acidic and basic functional groups varies with the bulk pH. Bulk ionic concentration enhances as pH deviates from 7. For lower values of N_A, the mobility reduces as the salt concentration is enhanced. However, the absolute value of the mobility enhances as the bulk concentration is enhanced when N_A is moderate. As C_{KCl} increases, a larger N_A is required to induce the counterion condensation, i.e. if N_A is large, the effect of CC is significant unless C_{KCl} is sufficiently high. Several experimental studies, as cited by Yeh et al. [12], found the similar trend in the variation of mobility with salt concentration. Yeh et al. [12] has provided a detailed analysis on the dependence of mobility on salt concentration at different pH.

4.4 Ion partitioning effect on mobility

The ion partitioning creates a modification in the distribution of mobile ions in the PE compared to the situation in which the dielectric permittivity of both the medium are same. If the permittivity of the PE is less than that of the electrolyte, the hydrogen/hydroxide ions prefer to remain inside the electrolyte rather than the PE, which leads to more ionization of acidic/basic groups relative to the case when the permittivities of the two mediums are the same. Thus, the volumetric charge density of the PE enhances as the permittivity of PE becomes lower than the electrolyte medium. When the PE is in electrophoresis the ion transport within the PE is screened by the ion partitioning effect. A decrease in concentration of counterions in PE lowers the shielding effect of the PE charge as well as reduces the DLP effect. These two in combination may enhance the mobility by enhancing the electric force experienced by the PE. It is evident from Fig. 3B, C, and Fig. 4A that a decrease in the PE-to-electrolyte permittivity ratio (ε_r) produces an enhancement in the mobility of the PE. The intensification in mobility due to the variation of ε_r is more pronounced for softer (lower β) PE as well as higher electrolyte concentration. As the PE become more permeable (lower β) the EOF of the counterions in and around the PE becomes more pronounced as well as the shielding effect of PE charge reduces, which creates an enhancement in the effective charge density of PE as β becomes lower. Thus, a high permeable PE (low β) attracts more counterions. For this, the effect of ε_r manifests for lower values of β. Similar argument can be made to justify the enhanced impact of ε_r

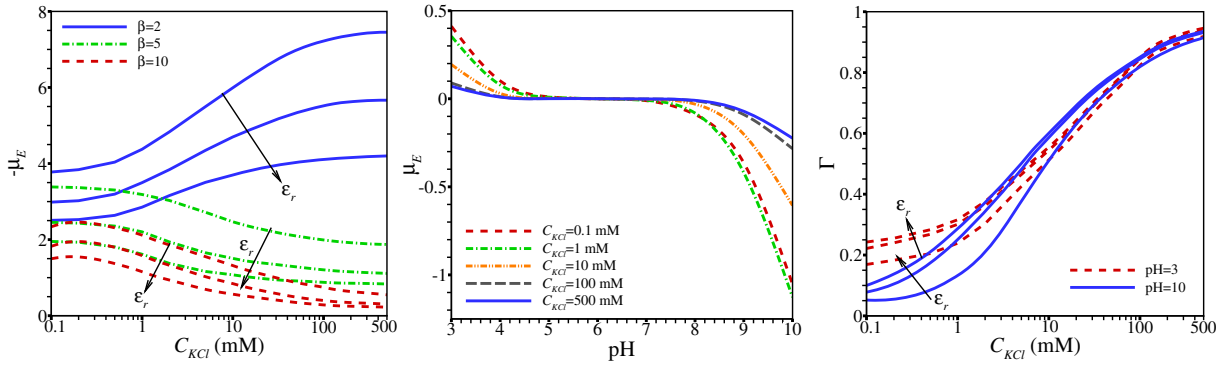

Figure 4. Variation of mobility (A) with C_{KCl} for different β (= 2, 5, 10) and different ε_r (= 0.5, 0.75, 1) at pH = 10 and (B) with pH for different C_{KCl} (= 0.1, 1, 10, 100, 500) at $\varepsilon_r = 1$ and β = 10 when $N_A = N_B = 50$ mM; (C) Variation of neutralization factor, Γ with C_{KCl} at $N_A = N_B = 100$ mM for different ε_r (= 0.5, 0.75, 1) and different pH (= 3, 5, 8, 10) when β = 2.

on μ_E at larger values of the salt concentration. Impact of the ion partitioning effect amplifies as pH deviates from IEP as for these pH the PE charge density becomes larger and more counterions from the electrolyte medium are attracted. Figure 4C shows that the charge neutralization factor Γ of the PE is higher at higher values of the PE-to-electrolyte permittivity ratio. This implies that the neutralization of the PE immobile charge occurs at a slower rate when PE have lower permittivity ($\varepsilon_r < 1$).

Distribution of counterions in and around the PE for different values of the PE-to-electrolyte permittivity ratio is illustrated in Fig. 5. We have presented the result for the moderate value of the salt concentration such that $\kappa a = 0.463$ for which the DLP effect is strong. The double layer polarization is evident from the figures. The results show that the concentration of the counterions within the PE becomes lower as ε_r is reduced. As mentioned previously, the Born energy difference of ions across the two medium of different dielectric permittivity creates an ion partitioning effect. This leads to a stronger polarization of the double layer as well as a lower screening of PE charge for lower values of ε_r. The polarization of the double layer creates a retardation of the induced electric field. However, μ_E becomes larger with the reduction of ε_r as the effective charge density of the PE rises, as discussed before. The streamline patterns are also indicated in Fig. 5. It shows a Stokes flow pattern around the PE.

The impact of the volume density of functional groups and screening length of the PE on the mobility for different choice of PE dielectric permittivity is presented in Fig. 6A and B. Increase in N_A produces a larger charge density of the PE, which creates an enhancement in the Donann potential and hence, an increased mobility. Results show that μ_E increases with the increase of N_A and approaches a saturation for larger value of N_A. Increase in N_A creates a stronger shielding effect as well as a DLP effect. These retarding effects are balanced with the enhanced electric force to create a constant μ_E for a larger range of N_A. The impact of ε_r is pronounced as the PE charge density is increased. Reduction in screening length of the PE creates a reduction in the mobility. The impact of the dielectric permittivity ratio is found to be significant for higher range of hydrogel screening length (i.e. lower β). The impact of the convective transport of ions in PE is significant for lower values of β. For this the impact of ion screening effect is pronounced for lower range of β. For low permeable PE (higher β), the ion transport is dominated by the linear diffusion mechanism.

The distribution of potential along the surface of the PE at different choice of ε_r is depicted in Fig. 7A. A decrease in the concentration of the counterions for lower permittivity of the PE creates an enhancement in electric potential around the PE. For lower ε_r, an asymmetric distribution in the surface potential ϕ_s is found. This asymmetry in ϕ_s is due to the polarization of double layer, which creates a retarding induced electric field acting opposite to the direction of the particle translation. It is evident that the polarization effect is stronger for lower ε_r. As the ion partitioning effect becomes stronger, the counterion condensation effect diminishes and the DLP effect intensifies. This is evident from the distribution of the surface potential.

We now measure the hindrance created by the double layer on migration of the PE. The ratio of drag between a charged nanogel in electrophoresis and the corresponding uncharged nanogel translating at the identical velocity U_E in the same medium is determined by the factor **Ω**. The hydrodynamic drag on an uncharged nanogel can be obtained as [38]

$$F_D^H = \frac{2\beta^2[1-(\tanh\beta/\beta)]}{2\beta^2+3[1-(\tanh\beta/\beta)]}6\pi U_E \tag{17}$$

In Fig. 7B we have shown the variation of **Ω** with salt concentration at different dielectric permittivity ratio. When PE is in electrophoresis, the unbalanced counterions in and around the PE creates a retarding electric body force and thus, the drag is higher compared to the hydrodynamic case obtained by Eq. (17), and because of this the drag ratio **Ω** is bigger than 1. The drag factor decreases with the rise of salt concentration, i.e. the decrease of Debye length. Higher salt concentration attenuates the retarding DLP effect. For this **Ω** approaches 1

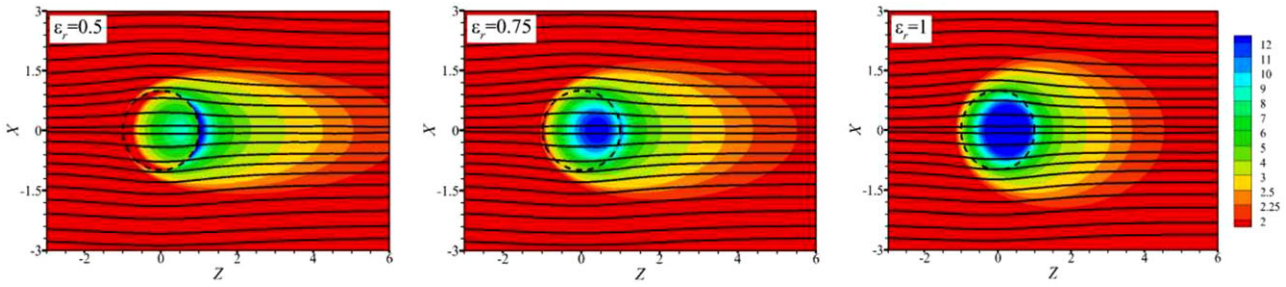

Figure 5. Streamlines and counterion distribution around and within the nanogel for $\varepsilon_r = 0.5$, 0.75, and 1 at pH = 10 when $C_{KCl} = 0.1$ mM, $N_A = N_B = 100$ mM, and $\beta = 2$. Dashed circle represents the surface of the nanogel.

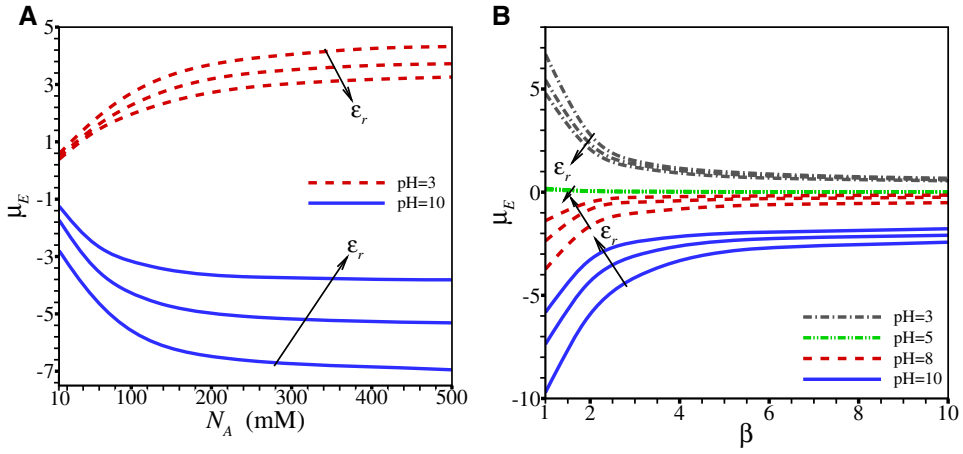

Figure 6. Variation of mobility for different ε_r (= 0.5, 0.75, 1) and different pH (A) with N_A for $N_A = N_B$ at $\beta = 2$ and (B) with β at $N_A = N_B = 100$ mM when $C_{KCl} = 1$ mM.

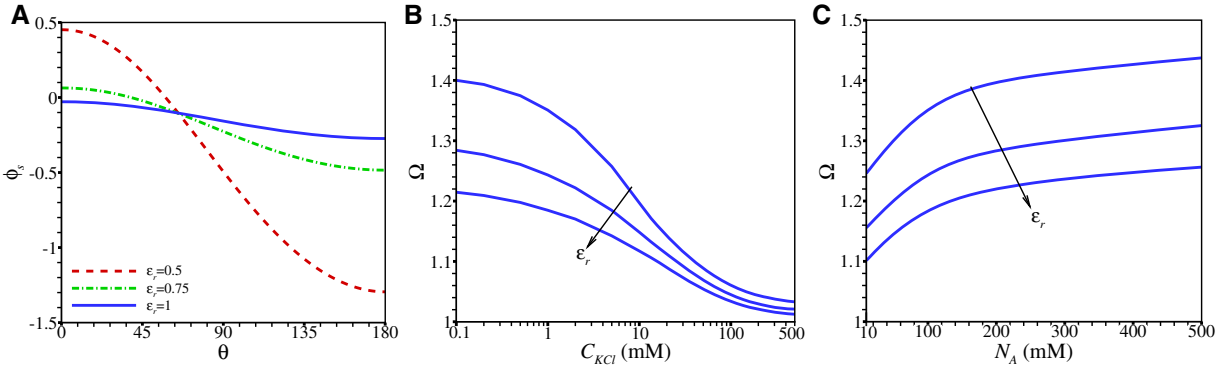

Figure 7. (A) Induced potential distribution on the surface of the nanogel at $C_{KCl} = 100$ mM for different ε_r (= 0.5, 0.75, 1). Variation of drag ratio between the charged and uncharged nanogel ($\Omega = F_D/F_D{}^H$) for different ε_r (= 0.5, 0.75, 1) with (B) C_{KCl} at $N_A = N_B = 100$ mM and (C) N_A for $N_A = N_B$ at $C_{KCl} = 1$ mM, when pH = 10 and $\beta = 2$.

as ionic concentration of the electrolyte becomes sufficiently large, i.e. $\kappa a >> 1$. The drag factor increases with the increase of the concentration of PE functional group. Higher charge density of the PE attracts more counterions due to the shielding effect, which creates a stronger EOF opposite to the direction of motion of the PE. Both the Fig. 7B, C shows that the drag factor increases as the PE-to-electrolyte permittivity ratio (ε_r) is decreased. As illustrated in Fig. 7 the DLP effect intensifies as ε_r is reduced, which leads to an enhanced drag for lower values of ε_r. Thus the hindrance created by the unbalanced counterions attenuates as the permittivity of the PE becomes closer to the electrolyte.

A nonlinear dependence of the PE electrophoretic velocity on the applied electric field is evident from the Fig. 8A. The impact of ε_r is larger for larger E_0. In Fig. 8A we have computed the mobility $\kappa a = 1.086$, for which the convective transport of ions is important. A stronger applied electric field produces a larger EOF induced by the unbalanced counterions, which leads to a stronger retardation effect. For this, we find a nonlinear variation of the mobility with the

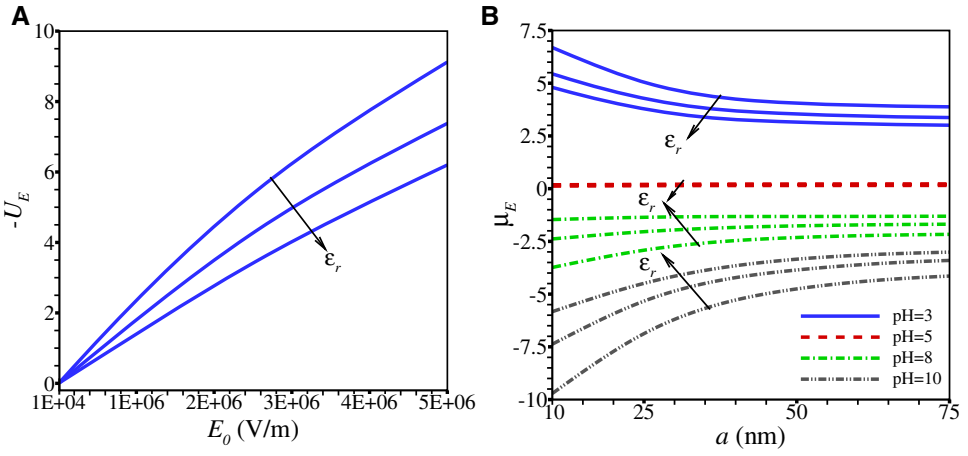

Figure 8. (A) Variation of electrophoretic velocity with the external electric field (E_0) for different ε_r (= 0.5, 0.75, 1) at pH = 10 when $C_{KCl} = 1$ mM, $N_A = N_B = 100$ mM and $\beta = 2$; (B) Variation of mobility with nanogel radius for different pH (= 3, 5, 8, 10) and different ε_r (= 0.5, 0.75, 1) at C_{KCl} = 1 mM when $N_A = N_B = 100$ mM and $\ell = 10$ nm.

applied electric field. The impact of the Joule heating may become pronounced at a higher range of the applied electric field. Joule heating creates a decrease in the buffer viscosity and hence, modifies the resistance of the buffer to the current flow in the medium. Joule heating is lower for the lower range of salt concentration as it creates lower current in the medium. We have presented results for lower ionic concentration and moderate range of the applied field strength, i.e. $\Lambda \leq 2$. The considered range of the applied electric field ($\Lambda \leq 2$) at $\kappa a = 1.086$ implies that the field creates a potential drop across the Debye layer in the order of the thermal potential. Thus, it is expected that the Joule heating will not be significant for the considered range of parameter values.

An increase in PE size, keeping other electrostatic parameter fixed, causes the net charge of the PE to increase, but produces an enhancement in DLP and relaxation effects. This retarding DLP and relaxation effects have stronger impact on lower range of the bulk ionic concentration, i.e. $\kappa a \sim O(1)$. For this a nonlinear dependence of μ_E with the increase of a occurs for the lower range of κa. For higher range of the size a, the mobility approaches a saturation. The theoretical analysis [16,39] shows that for $\kappa a >> 1$ mobility approaches a constant Q_{fix}/β^2. Increase in size a increases the net charge of the PE as well as decreases the permeability parameter β. The PE charge density is scaled by the square of the particle size whereas β is scaled by a^2, thus, Q_{fix}/β^2 becomes independent of a. This justifies the occurrence of saturation in mobility at a larger value of the particle size a as depicted in Fig. 8B.

5 Concluding remarks

We consider the electrophoresis of a pH-regulated polyelectrolyte nanogel (PE) by considering the ion partitioning effect arises due to the difference in dielectric permittivity of the nanogel and the surrounding electrolyte medium. The PE contains both acidic and basic functional groups, which create positive, negative, or zero charge depending on the bulk pH of the electrolyte and consequently, the mobility reversal can be achieved by varying the bulk pH. The PE charge and hence, the mobility enhances as the pH deviates from the iso-electric point. The magnitude of PE mobility enhances as the salt concentration is increased.

The ion partition effect enhances the ionization of PE functional group to create an enhanced PE charge. The counterion penetration in the PE attenuates if the permittivity of the PE is lower than the electrolyte medium. The reduced shielding effect leads to an enhanced mobility when the permittivity of the PE is lower than the electrolyte medium. The impact of this partitioning effect is prominent at higher values of the salt concentration and/or larger concentration of PE functional groups. The polarization of the ionic cloud around the PE becomes stronger as the ion partitioning effect attenuates counterion penetration in the PE. This creates an asymmetry in the electric potential distribution at the surface of the PE and a stronger hindrance on migration of the PE.

The present study confirms that the ion partitioning effect arising due to the difference in permittivity of PE from the electrolyte medium has a nonnegligible impact on electrophoresis of the PE. This effect enhances the nonlinear polarization effects and attenuates the counterion condensation effect on the electrophoresis, which may not be analyzed based on a linear or first-order perturbation analysis.

One of the authors (S.B.) acknowledges the financial support received from the Science & Engineering Research Board, Govt. India through the Project Grant No. EMR/2016/000185.

The authors have declared no conflict of interest.

6 References

[1] Viovy, J.-L., *Rev. Mod. Phys.* 2000, *72*, 813.

[2] Chen, Y.-Y., Hsu, J. -P., Tseng, S., T. J., *J. Colloid Interface Sci.* 2014, *421*, 154–159.

[3] Ballhause, D., Wallmersperger, T., *Smart Mater. Struct.* 2008, *17*, 045011.

[4] Hoagland, D. A., Arvanitidou, E., Welch, C., *Macromolecules* 1999, *32*, 61806190.

[5] Yeh, L.-H., Liu, K.-L., Hsu, J.-P., *J. Phys. Chem. C* 2011, *116*, 367–373.

[6] Ohshima, H., *J. Colloid Interface Sci.* 1994, *163*, 474–483.

[7] Ohshima, H., *Electrophoresis* 2006, *27*, 526–533.

[8] Duval, J. F. L., Ohshima, H., *Langmuir* 2006, *22*, 3533–3546.

[9] Yeh, L.-H., Hsu, J.-P., *Soft Matter* 2011, *7*, 396–411.

[10] Ohshima, H., *Soft Matter* 2012, *8*, 3511–3514.

[11] Huang, C.-H., *Phys. Chem. Chem. Phys.* 2012, *14*, 657–667.

[12] Yeh, L.-H., Tai, Y.-H., Wang, N., Hsu, J.-P., Qian, S., *Nanoscale* 2012, *4*, 7575–7584.

[13] Yameen, B., Ali, M., Neumann, R., Ensinger, W., Knoll, W., Azzaroni, O., *Nano Lett.* 2009, *9*, 2788–2793.

[14] Hou, X., Liu, Y., Dong, H., Yang, F., Li, L., Jiang, L., *Adv. Mater.* 2010, *22*, 2440–2443.

[15] Hermans, J. J., *J. Polym. Sci. A* 1955, *18*, 527–534.

[16] Hermans, J. J., *Koninkl. Ned. Akad. Wetenschap. Proc.* 1955, *58*, 182–187.

[17] Ohshima, H., *Colloids Surf. A* 1995, *103*, 249–255.

[18] Hsu, H.-P., Lee, E., *J. Colloid Interface Sci.* 2013, *390*, 85–95.

[19] He, Y.-Y., Lee, E., *Chem. Eng. Sci.* 2008, *63*, 5719–5727.

[20] Hsu, J. P., Lin, C.-Y., Yeh, L.-H., Lin, S.-H., *Soft Matter* 2012, *8*, 9469–9479.

[21] Manning, G. S., *J. Phys. Chem. B* 2007, *111*, 8554–8559.

[22] Hsu, H.-P., Lee, E., *Electrochem. Commun.* 2012, *15*, 59–62.

[23] Bhattacharyya, S., Gopmandal, P. P., *Soft Matter* 2013, *9*, 1871–1884.

[24] Jim´enez, M. L., Bellini, T., *Curr. Opin. Colloid Interface Sci.* 2010, *15*, 131–144.

[25] Duval, J. F. L., Gaboriaud, F., *Curr. Opin. Colloid Interface Sci.* 2010, *15*, 184–195.

[26] Andrews, J., Das, S., *RSC Adv.* 2015, *5*, 46873–46880.

[27] Ganjizade, A., Ashrafizadeh, S. N., Sadeghi, A., *Electrochem. Commun.* 2017, *84*, 19–23.

[28] Young, M. A., Jayaram, B., Beveridge, D. L., *J. Phys. Chem. B* 1998, *102*, 7666–7669.

[29] Coster, H. G. L., *Biophys. J.* 1973, *13*, 133–142.

[30] L´opez-Garc´ıa, J. J., Horno, J., Grosse, C., *J. Colloid Interface Sci.* 2003, *268*, 371–379.

[31] Ganjizade, A., Sadeghi, A., Ashrafizadeh, S. N., *Colloids Surf. B* 2018, *170*, 129–135.

[32] Maurya, S. K., Gopmandal, P. P., Bhattacharyya, S., Ohshima, H., *Phys. Rev. E* 2018, *98*, 023103.

[33] Israelachvili, J. N., *Intermolecular and Surface Forces*. Academic Press, Cambridge, Massachusetts 2011.

[34] Switzer, R. L., Garrity, L. F., *Experimental Biochemistry*. W. H. Freeman Publishing, New York, USA 1999.

[35] Nightingale Jr., E. R., *J. Phys. Chem.* 1959, *63*, 1381–1387.

[36] Duval, J. F. L., Slaveykova, V. I., Hosse, M., Buffle, J., Wilkinson, K. J., *Biomacromolecules* 2006, *7*, 2818–2826.

[37] Yeh, L.-H., Hsu, J.-P., Qian, S., Tseng, S., *Electrochem. Commun.* 2012, *19*, 97–100.

[38] Neale, G., Epstein, N., Nader, W., *Chem. Eng. Sci.* 1973, *28*, 1865–1874.

[39] Keh, H. J., Chen, W. C., *J. Colloid Interface Sci.* 2006, *296*, 710–720.

